Int. J. Electrochem. Sci., 10 **(2015)** 2045 - 2054

International Journal of
ELECTROCHEMICAL
SCIENCE
www.electrochemsci.org

Short Communication

Effect of Sn Content on the Corrosion Behavior of Ti-based Biomedical Amorphous Alloys

X.Q. Wu, Q. Peng, J.C. Zhao, J.G. Lin[*]

[1] School of Material Science and Engineering, Xiangtan University, Xiangtan, Hunan, 411105, PR China.
[2] Key Laboratory of Low Dimensional Materials & Application Technology (Xiangtan University), Ministry of Education, PR China.
[*]E-mail: lin_j_g@163.com

Received: 28 November 2014 / *Accepted:* 16 December 2014 / *Published:* 19 January 2015

The $(Ti_{60}Zr_{10}Ta_{15}Si_{15})_{100-x}Sn_x$ (x=0, 4, 8, 12 at. %) ribbons were prepared by using the single roll melt-spinning method, and the fully amorphous alloys were obtained in the alloys as the Sn content increasing from 0 to 8 at. %. The effects of the Sn addition on the corrosion behavior of the amorphous alloys in phosphate buffer solution (PBS) were investigated using electrochemical polarization and electrochemical impedance spectroscopy (EIS) tests. The results show that the amorphous alloys exhibit the passivated characterization with the formation of a stable passive film on their surfaces during the immersion in PBS solution, and thus they have a superior corrosion resistance in the PBS solution in comparison with the pure Ti and the crystalline $Ti_{60}Zr_{10}Ta_{15}Si_{15}$ alloy. The addition of Sn into the amorphous $Ti_{60}Zr_{10}Ta_{15}Si_{15}$ decreases the passive current density. The corrosion resistance of the amorphous alloys increases with the Sn content increasing from 0 to 8 at. %.

Keywords: Titanium alloys, Biomedical amorphous materials, Corrosion resistance

1. INTRODUCTION

Titanium and its alloys are often used as biomaterials to replace or repair structural components of the human body in the field of trauma and orthopedic surgery [1]. Despite the high rates of success with these Ti-based implant materials, there are still serious problems with regard to safety and long-term durability in the human body [2]. One of the major problems is the mismatch of the Young's modulus (E) values between the bone (E=10-30 GPa) and the implant (E=110-120 GPa for commercially pure cp-Ti and Ti–6Al–4V alloys) [3]. It can cause insufficient loading of bone adjacent

to the implant, resulting in the stress-shielding effects that cause tissue loss and implant failure [4]. Another notable problem is the release of toxic metallic ions and/or particles through the corrosion and wear processes that lead to inflammatory cascades, which reduce the biocompatibility [5]. Therefore, a lot of research is currently being undertaken, dedicating to the development of new titanium alloys with improved biological and biomechanical properties.

In recent years, bulk metallic glasses (BMGs) have been widely investigated owing to their high strength and hardness, low Young's modulus, excellent corrosion resistance, and excellent formability that allows the production of precise and versatile geometries on scales of length ranging from tens of nanometers to several centimeters, which is of great interest for biomaterials processing [6]. Ti-based BMGs have attracted huge interest for use in the biomedical field since they possess better characteristics than their crystalline counterparts [7]. However, many elements that favor glass formation are not necessarily biologically compatible, which then puts constraints on the alloy design of biocompatible glassy alloys. For example, Ni and Cu are commonly found in Ti-based BMGs [8, 9]. However, both elements are highly allergenic and/or toxic while Ni is possibly carcino-genic and should be avoided in implant applications [10]. The breakthrough in biocompatible Ti-BMG research came with the discovery of Ni-free $Ti_{40}Zr_{10}Cu_{36}Pd_{14}$ glass formers by Inoue and coworkers at Tohoku University [11]. These new bulk glassy alloys exhibit excellent glass-forming ability, but the Ni-free Ti-based BMGs still have some weak points. For example, these Ti-based BMGs contain a large amount of Cu, which is a highly cytotoxic element [12]. Furthermore, they are highly sensitive to pitting corrosion due to the combination of Ti and Cu [13]. In the development of biocompatible Ti-based metallic glasses, free of Ni and Cu, notable progress has been reported recently by Oak et al [14], who produced fully amorphous ribbons in Ti-Zr-Ta-Si systems. However, the forming ability of the amorphous alloy is lower than that of the $Ti_{40}Zr_{10}Cu_{36}Pd_{14}$ alloy developed by Inoue [11].

On the other hand, as a candidate of body implant materials, its corrosion properties in the body fluid should be evaluated, because the release of the ions from the implant to the surrounding tissues may give rise to the biocompatibility problems. So, many attempts have devoted to improve the corrosion resistance of the Ti-based alloys for biomedical use [15-18]. It has been well documented that the corrosion resistance of Ti alloys can be improved by adding some alloying elements. It has been found that the addition of the Zr and Mo into the Ti-22Nb alloy can improve the corrosion resistance of the alloy in the NaCl solution [19], while the Sn addition can promote the corrosion resistance of TiTa alloys [20], and the Si addition to the TiNb alloy can increase its mechanical resistance and without negatively influencing on the corrosion resistance [21]. In addition, the surface modification is another way to improve the corrosion resistance of an alloy. For example, it has been reported that the surface modificated Ti-6Al-4V alloy showed enhanced corrosion resistance [22]. Moreover, the Ti alloys with the amorphous structure exhibits superior corrosion resistance in comparison with their crystalline counterpart, and the microstructure feathers, such as the homogeneous chemical composition and the crystal defect-free, may be responsible for their excellent corrosion behavior [8]. It is well known that an amorphous alloy usually contains several alloying elements, and how the alloying elements affect the corrosion behavior needs to be further clarified.

In the present work, the novel Ti-based amorphous alloys $(Ti_{60}Zr_{10}Ta_{15}Si_{15})_{100-x}Sn_x$ (x=0, 4, 8, 12 at. %) were prepared by using spinning method, and the electrochemical corrosion behavior of the

alloys in PBS solution were investigated, focusing on the effects of Sn content on the corrosion resistance of the alloys.

2. MATERIALS AND METHODS

2.1 Materials and experimental procedure

Master alloys with nominal compositions of $(Ti_{60}Zr_{10}Ta_{15}Si_{15})_{100-x}Sn_x$ (x=0, 4, 8, 12 at. %) were prepared by arc melting from mixtures of pure metals of titanium, zirconium, tantalum, silicon and stannum in an argon atmosphere. To achieve fully amorphous structures, rapidly solidified thin ribbons with a thickness of approximately 40 μm and width of 1 mm were produced in melt spinning equipment at a speed of 35 m s^{-1} in an argon atmosphere. The structure of ribbons was examined by X-ray diffraction (XRD) using Cu Kα radiation.

2.2 Electrochemical characterization

The electrolyte of phosphate buffer solution (PBS) with a pH value of 7.44 was chosen for the simulated human body liquid. Its composition is: NaCl (8 g L^{-1}), KCl (0.2 g L^{-1}), Na_2HPO_4 (1.12 g L^{-1}), KH_2PO_4 (0.2 g L^{-1}) [14]. The corrosion resistance of the amorphous Ti-based alloy ribbons was evaluated through electrochemical measurements and impedance spectroscopy (EIS) tests. For comparison, the corrosion resistance of the commercial pure Ti (Ti Grade 2) and $Ti_{60}Zr_{10}Ta_{15}Si_{15}$ crystalline alloy was also evaluated in the same corrosion medium. Prior to the corrosion tests, the specimens were mechanically polished with silicon carbide paper up to grit 2000, degreased in acetone, washed in distilled water, dried in air, and further exposed to air for 24 h for good reproducibility. Electrochemical measurements were conducted in a three-electrode cell using a platinum counter electrode and an Ag/AgCl reference electrode. Potentiodynamic polarization curves were measured at a potential sweep rate of 0.167 mV s^{-1}, the amplitude of EIS tests was 5 mV at open circuit potential, and the frequency ranged from 10^5 Hz to 10^{-2} Hz. The electrochemical tests were carried out according to ASTM G-16. Before the electrochemical measurements, the samples were immersed in the solutions for about 40 min when the open-circuit potential became steady. The test for each sample was repeated six times.

3. RESULTS AND DISCUSSION

3.1 Microstructures

Fig. 1 shows the XRD patterns of the as-spun $(Ti_{60}Zr_{10}Ta_{15}Si_{15})_{100-x}Sn_x$ (x=0, 4, 8 and 12 at. %) ribbons. Only a broad peak within the diffraction angle 2θ in the range 35-45°appears on the XRD patterns of the alloy ribbons with Sn concentrations ranging from 0 to 8 at. %, indicating that ribbons

with a fully amorphous structure are successfully obtained in these alloys. However, the XRD pattern of the $(Ti_{60}Zr_{10}Ta_{15}Si_{15})_{88}Sn_{12}$ exhibits some diffraction peaks, which are identified to be ZrSi, Sn and TiSi phases.

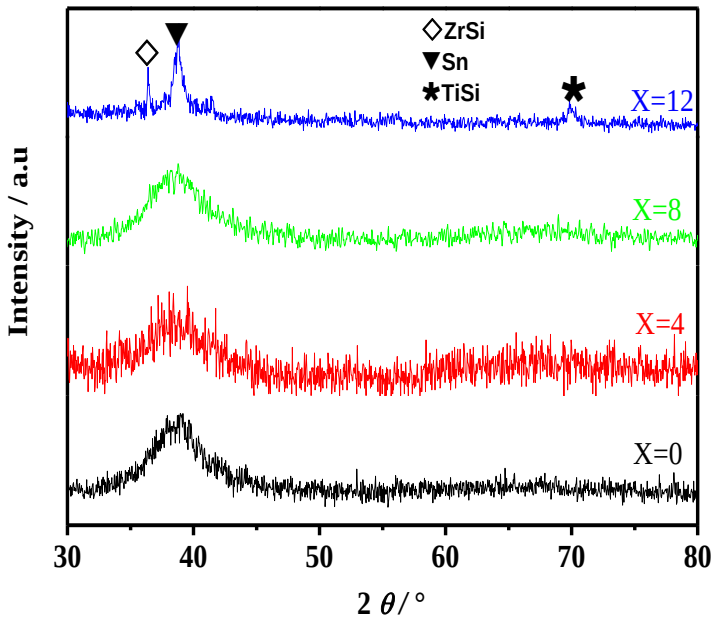

Figure 1. XRD patterns of the as-spun$(Ti_{60}Zr_{10}Ta_{15}Si_{15})_{100-x}Sn_x$ (x=0, 4, 8, 12 at. %) alloys.

So, the addition of Sn decreases the glass formation ability of $Ti_{60}Zr_{10}Ta_{15}Si_{15}$ alloy, and it is hard to obtain the fully amorphous alloy by using the single roll melt-spinning method as the addition of Sn is up to 12 at. %.

3.2 Polarization results

The corrosion behavior of the completely amorphous ribbons and commercial pure Ti and crystalline $Ti_{60}Zr_{10}Ta_{15}Si_{15}$ alloy were investigated in this study. Fig. 2 shows their potentiodynamic polarization curves in PBS solution at 310 *K* opened to air. The corrosion current densities were evaluated by extrapolating the cathodic branches back to the corrosion potentials. The potential range used for Tafel extrapolating is about 120-250 mV more negative than the corrosion potential because the cathodic branches have good linear regions in this potential range. The corrosion data, including the corrosion potential (E_{corr}), corrosion current density (I_{corr}), the cathodic Tafel slope (b_c) and critical passive current density (I_p) are gathered in Table 1. From Fig. 2 and Table 1, one can see that the commercial pure Ti exhibits the lowest E_{corr} (-0.403±0.007 V), and the highest $\boldsymbol{I_{corr}}$ (0.0331±0.0052 μA cm^{-2}), indicating that it is susceptible to corrosion in PBS solution, and yields the highest corrosion rate once the corrosion occurs among these samples. The cathodic Tafel slope (b_c) is found to be more or less the same for these amorphous ribbons. whereas commercial pure Ti has distinctly different cathodic Tafel slope. This phenomenon suggests that pure Ti shows different hydrogen evolution

behaviour compared with the other Ti alloys during cathodic polarization. It can also be seen that all the samples exhibit passivated characterization. The critical passive current density (I_p) of commercial pure Ti is about 2.120±0.123 μA cm^{-2}, which is very close to the I_p of 2.22 μA cm^{-2} reported in Bai's work [23].

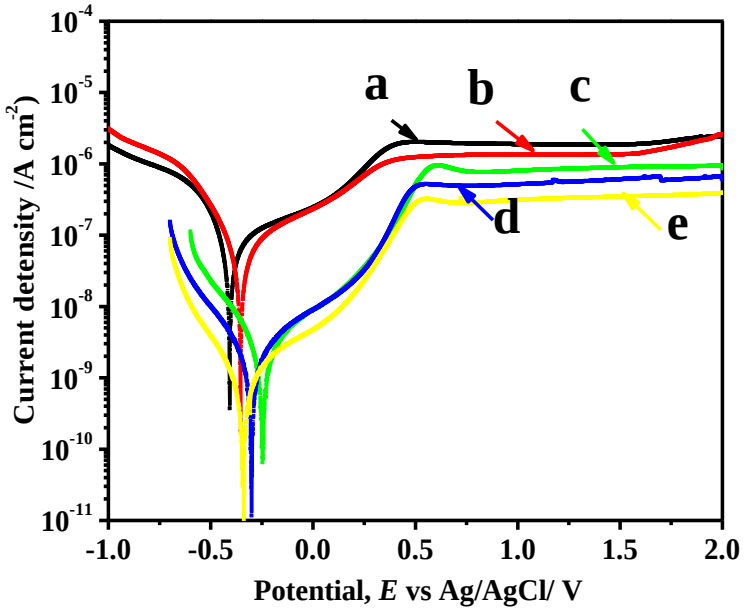

Figure 2. The potentiodynamic polarizationcurves of Ti and Ti alloys in PBS aqueous solutions. a, commercial pure Ti, b, crystalline $Ti_{60}Zr_{10}Ta_{15}Si_{15}$, c, amorphous $Ti_{60}Zr_{10}Ta_{15}Si_{15}$, d, amorphous $(Ti_{60}Zr_{10}Ta_{15}Si_{15})_{96}Sn_4$, e, amorphous $(Ti_{60}Zr_{10}Ta_{15}Si_{15})_{92}Sn_8$

Table 1. Results of the potentiodynamic polarization measurements in PBS solution. a, commercial pure Ti, b, crystalline $Ti_{60}Zr_{10}Ta_{15}Si_{15}$, c, amorphous $Ti_{60}Zr_{10}Ta_{15}Si_{15}$, d, amorphous $(Ti_{60}Zr_{10}Ta_{15}Si_{15})_{96}Sn_4$, e, amorphous $(Ti_{60}Zr_{10}Ta_{15}Si_{15})_{92}Sn_8$

Sample	E_{corr} / V	I_{coor} / $\times 10^{-1}$ μA cm^{-2}	b_c / mV dec^{-1}	I_p / μA cm^{-2}
a	-0.403±0.007	0.331±0.052	-217.4	2.120±0.123
b	-0.357±0.006	0.291±0.022	-172.7	1.701±0.112
c	-0.248±0.016	0.025±0.004	-169.4	0.982±0.025
d	-0.292±0.008	0.016±0.002	-174.8	0.523±0.024
e	-0.334±0.011	0.011±0.002	-176.7	0.321±0.028

The I_p of as spun $Ti_{60}Zr_{10}Si_{15}Ta_{15}$ alloy (0.982±0.025 μA cm^{-2}) is very close to that (about 1 μA cm^{-2}) of work reported by Oak and Inoue [14]. The I_p of commercial pure Ti is higher than that of the crystalline $Ti_{60}Zr_{10}Ta_{15}Si_{15}$ (I_p=1.701±0.112 μA cm^{-2}), which indicates the better corrosion resistance of the crystalline $Ti_{60}Zr_{10}Ta_{15}Si_{15}$ alloys than the commercial pure Ti in PBS solution. The amorphous alloy exhibits the superior corrosion resistance in comparison with the pure Ti and the crystalline alloy.

Moreover, the addition of Sn has a significant influence on the corrosion behavior of the $Ti_{60}Zr_{10}Ta_{15}Si_{15}$ amorphous alloy. With the Sn content increasing from 0 to 8 at. % , the value of I_p of the amorphous alloy decreases from 0.982±0.025 μA cm^{-2} to 0.321±0.028 μA cm^{-2}. It means that the Sn addition promotes the formation of more protective passive films on the surface of the amorphous alloy.

It should be noted that the potentiodynamic polarization curves for all the samples show a broad and distinctive passivation region. It implies that the passive films on the surface of the samples are stable and protective, which favors the protection of the alloy surface from corrosion. It has been well documented that an active-passive metal exposed to a corrosive medium yields the current density lower than about 100 μA cm^{-2} will be spontaneously passivated [24]. In the case of the present work, all the alloys were easily passivated in PBS solution, as evidenced by the low corrosion current density and low passive current density. Thus, they show a promising potential for biomedical applications in view of their high corrosion resistance in PBS.

3.3 EIS measurements and equivalent circular analysis

To further study the corrosion mechanisms of the alloys in PBS solution, the impedance measurements were performed in order to obtain detailed information about the corrosion behavior of the Ti and Ti alloys in PBS solution. The Nyquist diagrams and the Bode plots are shown in Fig. 3 (a) and (b), respectively. From Nyquist diagrams in Fig. 3, one can see that the impedance spectra of all the samples are characterized with a semicircle loop, implying that all the samples exhibit the same corrosion mechanism in the solution.

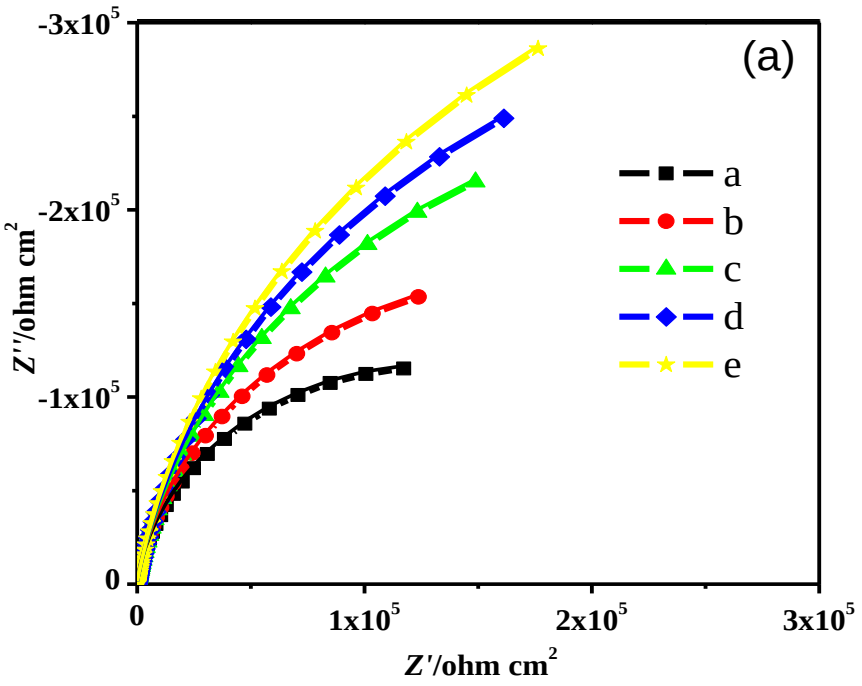

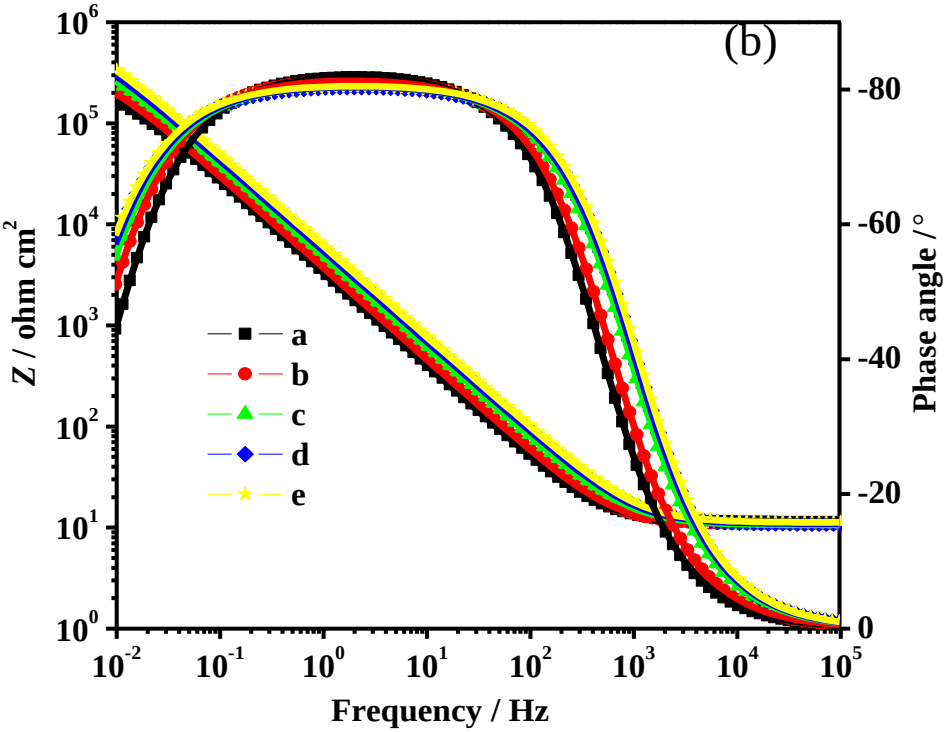

Figure 3. Experimental and simulated EIS diagrams obtained by the ZView software for the Ti and Ti alloys in PBS solution: (a) Nyquist plots, (b) Bode plots. (Line: fitted data; Symbol: experimental data). a, commercial pure Ti, b, crystalline $Ti_{60}Zr_{10}Ta_{15}Si_{15}$, c, amorphous $Ti_{60}Zr_{10}Ta_{15}Si_{15}$, d, amorphous $(Ti_{60}Zr_{10}Ta_{15}Si_{15})_{96}Sn_4$, e, amorphous $(Ti_{60}Zr_{10}Ta_{15}Si_{15})_{92}Sn_8$。

The appearance of the capacitive semicircle is associated with the formation of the oxide film capacitance on the surfaces of all the alloys. In comparison with pure Ti and the crystalline alloy, the amorphous alloys exhibit a bigger diameter of the capacitive loop on its impedance spectrum. Moreover, the diameter of the capacitive loop for the amorphous alloys increases with the Sn addition increasing, indicating that the Sn additions promote the impedance value of the alloys due to its more efficient passivity process.

Thus, the amorphous alloys exhibit higher corrosion resistance than pure Ti, and Sn addition further improves the corrosion resistance of the amorphous alloys. This result is in good agreement with that obtained from Fig. 2.

In order to obtain quantitative information about the EIS data, an equivalent circuit model was proposed in the present work. Considering all the Nyquist plots are characterized with a semicircle and the phase angle shows only one ‘‘peak’’ over the whole frequency range in the Bode plots for all samples, which is a typical nature of the single film on the surface of the alloys, an equivalent circuit model ($R_s(Q_pR_p)$), widely used for the fit of a single film on the surface of titanium alloys is adopted [25-26], as illustrated in Fig. 4.

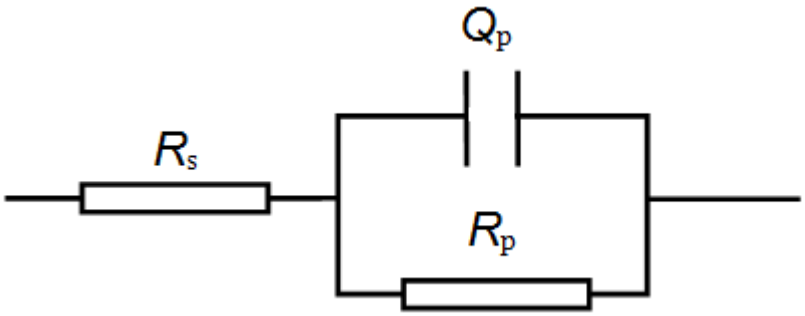

Figure 4. Equivalent circuit for modeling impendence parameters

In this model, R_s is the electrolyte resistance, R_p is the resistance of passive film, Q_p is the capacitance of constant phase element. The agreement between experimental and simulated results indicates that the experimental results are well fitted to the proposed equivalent circuit. The parameters (R_s, Q_p, n, and R_p) obtained by the fitting procedure are listed in Table 2. It is clear that the electrolyte resistance (R_s) has little change, but the passive film resistance (R_p) increases as the Sn content increases. The amorphous $(Ti_{60}Zr_{10}Ta_{15}Si_{15})_{92}Sn_8$ alloy is with the highest polarization resistance (8.65×10^5 ohm cm^2) and the lowest capacitance (30.86 μF cm^{-2}), implying that it exhibits the best corrosion resistance.

Table 2. Values of fitting parameters obtained using the $R_s(Q_pR_p)$ model to fit the experimental EIS data for the Ti and Ti alloys in PBS solution. a, commercial pure Ti, b, crystalline $Ti_{60}Zr_{10}Ta_{15}Si_{15}$, c, amorphous $Ti_{60}Zr_{10}Ta_{15}Si_{15}$, d, amorphous $(Ti_{60}Zr_{10}Ta_{15}Si_{15})_{96}Sn_4$, e, amorphous $(Ti_{60}Zr_{10}Ta_{15}Si_{15})_{92}Sn_8$

Sample	R_s / ohm cm^2	Q_p/ μF cm^{-2}	n	R_p / 10^5 ohm cm^2
a	11.4	54.50	0.91	2.64
b	10.8	49.47	0.91	3.81
c	10.6	38.32	0.89	5.97
d	10.9	34.38	0.89	7.26
e	11.2	30.86	0.89	8.65

4. CONCLUSIONS

In the present work, the $(Ti_{60}Zr_{10}Ta_{15}Si_{15})_{100-x}Sn_x$($x$=0, 4, 8, 12 at. %) ribbons were prepared by using the single roll melt-spinning method, and the fully amorphous ribbons were obtained in the alloys as the Sn contents range from 0 to 8 at. %. The electrochemical corrosion behaviors of the amorphous alloys in PBS solution were investigated by using EIS and potentiodynamic polarization

method in comparison with pure Ti and the crystalline $Ti_{60}Zr_{10}Ta_{15}Si_{15}$ alloy. The main conclusions are highlighted as follows.

(1) The amorphous alloys exhibit a superior corrosion resistance in comparison with pure Ti and the crystalline $Ti_{60}Zr_{10}Ta_{15}Si_{15}$ alloy, evidenced by their relatively high corrosion current density (I_{corr}) and the critical passive current density (I_p).

(2) Sn addition is conducive to the improvement of the corrosion resistance behavior of the amorphous alloys. With the Sn content increasing from 0 to 8 at. %, the corrosion current density (I_{corr}) and the passive current density (I_p) of the amorphous alloys decrease. The resistance of the passive film is increased by adding Sn into the amorphous $Ti_{60}Zr_{10}Ta_{15}Si_{15}$ alloy due to its more efficient passivity process.

ACKNOWLEDGMENTS
The authors would like to acknowledge the financial support of National Natural Science Foundation (11402220), the Education Department of Hunan Province (14B176), the Natural Science and Technology Foundation of Guizhou Province (No. LKS [2013] 43, No. Qian Ke He J Zi [2014] 2122).

References

1. M. Niinomi (ed), Metals for Biomedical Devices, CRC Press, Boca Raton (2010)
2. C. Leyens, M. Peters (eds), Titanium and Titanium Alloys, Wiley-VCH Verlag GmbH & Co. KGaA, Weinheim (2003)
3. M. Geetha, A.K. Singh, R. Asokamani, A.K. Gogia, *Prog. Mater. Sci*, 54 (2009) 397-425
4. M. Long, H.J. Rack, *Biomaterials*, 19 (1998) 1621-1639
5. Y. Okazaki, E. Gotoh, *Biomaterials*, 26 (2005)11-21
6. J. Schroers, G. Kumar, T.M. Hodges, S. Chan, T.R. Kyriakides, *JOM*, 61 (2009) 21-29
7. A. Inoue, Acta. Mater, 48 (2000) 279-306
8. C. Suryanarayana, A. Inoue, Bulk metallic glasses, CRC Press, Boca Raton (2011)
9. H.F. Hildebrand, J.C. Hornez, Biological Response and Biocompatibility, In: J.A. Helsen, H.J. Breme (Eds), Metals as Biomaterials, Wiley, Chichester (1998)
10. S.L. Zhu, X.M. Wang, F.X. Qin, A. Inoue, *Mater. Sci. Eng*., A, 459 (2007) 233-237
11. Waleed M. E, Ikuya. W, Phillip. K, *Dental Mater*, 25 (2009) 1551-1555
12. F.X. Qin, X. Wang, S. Zhu, A. Kawashima, K. Asami, A. Inoue, *Mater. Trans*, 48 (2007) 515-518
13. J. -J. Oak, A. Inoue, *Mater. Sci. Eng*., A, 449-451 (2007) 220-224
14. S. Yang, D. C. Zhang, M. Wei, H. X. Su, W. Wu and J. G. Lin, *Mater. Corros*, 64 (2013) 402-407
15. B. Guo, Y. X. Tong, F. Chen, Y. F. Zheng, L. Li and C. Y. Chung, *Mater. Corros*, 63 (2012) 259-263
16. S.C. Vanithakumari, R.P. George, and U. Kamachi Mudali, *Corrosion*, 69 (2013) 804-812
17. C.G. Nava-Dino, R.G. Bautista-Margulis, M.A. Neri-Flores, M.V. Orozco-Carmona, S.D de la Torre, J.G. Gonzalez-Rodriguez, J. G. Chacon-Nava, A. Martínez-Villafañe, *Int. J. Electrochem. Sci*., 7 (2012) 4250-4260
18. Y. L. Zhou, M. Niinomi, T. Akahori, H. Fukui, H. Toda, *Mater. Sci. Eng*., A, 398 (2005) 28–36
19. M. Atapour, A. Pilchak, G. S. Frankel, J. C. Williams, M. H. Fathi, and M. Shamania, *Corrosion*, 66 (2010) 065004-065004-9
20. S. Tamilselvi, R. Murugaraj, N. Rajendran, *Mater. Corros*, 58 (2007)113-120
21. N.T.C. Oliveira , A.C. Guastaldi, *Acta Biomater*, 5 (2009) 399-405

22. Y. Bai, Y.L. Hao , S.J. Li , Y.Q. Hao, R. Yang, F. Prima, *Mater. Sci. Eng*., C, 33 (2013) 2159-2167
23. Y. Bai, S.J. Li, F. Prima, Y.L. Hao, R. Yang, *Appl. Surf. Sci*, 258 (2012) 4035-4040
24. Y. F. Zheng, B. L. Wang, J. G. Wang, *Mater. Sci. Eng*., A, 438-440 (2006) 891-895
25. W. Osório, J. Spinelli, I. Ferreira, A. Garcia, *Electrochim. Acta*, 52 (2007) 3265-3273
26. M. Karthega, V. Raman, N. Rajendran, *Acta Biomater*, 3 (2007) 1019-1023